P H Y S I C A L   R E V I E W   L E T T E R S

Preparation of Ultracold Atom Clouds at the Shot Noise Level

M. Gajdacz,[1] A. J. Hilliard,[1,*] M. A. Kristensen,[1] P. L. Pedersen,[1] C. Klempt,[2] J. J. Arlt,[1] and J. F. Sherson[1]

[1]*Institut for Fysik og Astronomi, Aarhus Universitet, Ny Munkegade 120, 8000 Aarhus C, Denmark*
[2]*Institut für Quantenoptik, Leibniz Universität Hannover, Welfengarten 1, D-30167 Hannover, Germany*

We prepare number stabilized ultracold atom clouds through the real-time analysis of nondestructive images and the application of feedback. In our experiments, the atom number $N \sim 10^6$ is determined by high precision Faraday imaging with uncertainty ΔN below the shot noise level, i.e., $\Delta N < \sqrt{N}$. Based on this measurement, feedback is applied to reduce the atom number to a user-defined target, whereupon a second imaging series probes the number stabilized cloud. By this method, we show that the atom number in ultracold clouds can be prepared below the shot noise level.

Over the past decade, experiments with ultracold atomic samples have matured from the proof-of-concept level to a development platform for technologies such as quantum sensors and quantum simulators. One rapidly expanding technique is the manipulation of quantum systems using measurements and feedback [1–3]. To limit the backaction, usually a "weak" measurement is employed, such as detecting the phase shift induced by an atomic ensemble on an off-resonant laser beam [4]. Recent experiments have demonstrated feedback control of motion in an optical lattice [5], a quantum memory for light [6], deterministic spin squeezing [7], stabilization of an atomic system against decoherence [8], extending the interrogation time in Ramsey experiments [9], and feedback cooling of a spin ensemble [10].

To fully exploit the potential of ultracold clouds in emerging quantum technologies, these atomic samples must be prepared with unprecedented precision. For instance, precise atom number preparation is crucial to improving the precision of atomic clocks, which is presently limited by collisional shifts [11]. It is of particular relevance for techniques that employ interactions to produce nonclassical states for improved interferometric sensitivity [12–15]. In general, if the number fluctuations of an atomic ensemble in a single spatial mode can be suppressed, the many-particle state becomes nonclassical, yielding a resource for atom interferometry beyond the standard quantum limit [16]. Sub-Poissonian preparation of micro- and mesoscopic atomic samples was recently demonstrated by using single-site addressing in an optical lattice [17], three-body collisions [18,19], nondestructive measurements of nanofiber-based systems [20], and careful tailoring of the trapping potential for fermionic [21] and bosonic systems [22]. However, despite initial attempts towards the compensation of number fluctuations in ultracold atomic clouds [23], the high precision preparation of large atom numbers remains an unsolved challenge.

In this Letter, we stabilize the atom number in ultracold clouds through the real-time analysis of dispersive images

and feedback, as shown in Fig. 1(a). After initial evaporative cooling of an atomic cloud, a first set of nondestructive Faraday images $F1$ determines the number of atoms. We characterize this imaging method and show it achieves an atom number uncertainty below the shot noise level. Based on the analysis of the images, feedback is applied to reduce the atom number to a user-defined target, whereupon a second imaging series $F2$ probes the remaining number of atoms in the cloud. We show that this technique can stabilize the atom number below the shot noise level.

The evolution of the atom number distribution throughout the sequence can be understood as follows. The high
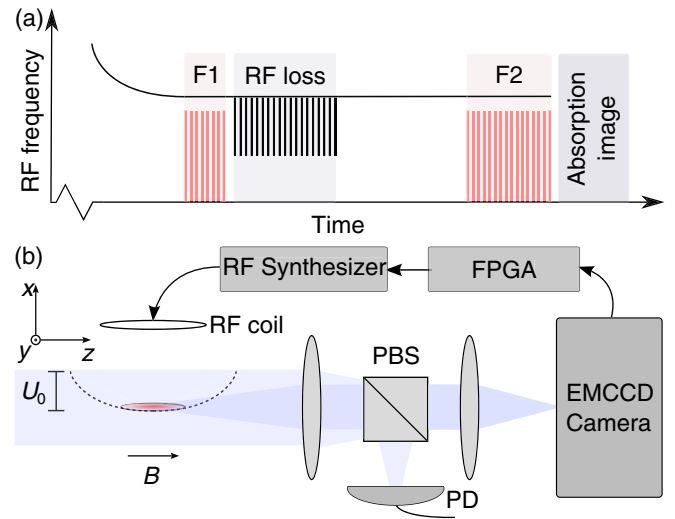

FIG. 1. (a) Experimental sequence. An evaporatively cooled cloud is probed by two series of Faraday images, where rf loss pulses between $F1$ and $F2$ remove a controllable fraction of the atom cloud. (b) Experiment schematic. Faraday imaging probes a cold atom cloud held in a magnetic trap. The images are processed in real time, and the outcome can be used to determine the fraction of atoms removed by rf loss, thereby producing a number stabilized cloud.

precision of the Faraday imaging sets the width of the atom number distribution at $F1$ below the shot noise level. To stabilize the atom number, a precise fraction of the atoms is removed from the cloud, causing the width of the atom number distribution to grow. In general, the loss process between $F1$ and $F2$ can be modeled by a master equation, the solution of which yields the probability distribution for the number of trapped atoms as a function of time [24]. For single-particle loss, however, the atom number distribution is Poissonian, which may be approximated by a binomial distribution for large N due to the central limit theorem. This motivates the following simplified model: Starting with N_0 atoms in the trap, where each atom has a probability p of remaining trapped, the number of remaining atoms has a binomial distribution $N \sim B(N_0, p)$, with mean value $\langle N \rangle = N_0 p$ and variance $N_0 p(1-p)$. Thus, the relative uncertainty of the number of atoms remaining in the cloud is given by $\sqrt{(1-p)/\langle N \rangle}$. From this simple analysis, it is clear that for low levels of applied loss ($p \simeq 1$), samples with a relative uncertainty well below the shot noise level $1/\sqrt{\langle N \rangle}$ can be prepared, provided feedback does not add additional noise.

Having outlined the sequence to stabilize the atom number, we now give a more detailed description of the experiment. Figure 1(b) shows a schematic of the key components in the experimental setup. Ultracold atomic clouds are produced by forced radio-frequency (rf) evaporation in an Ioffe-Pritchard magnetic trap. The trap has radial and axial trapping frequencies of $\omega_\rho = 2\pi \times 296$ Hz and $\omega_z = 2\pi \times 17.1$ Hz, at a 330 mG bias field. The rf evaporation is stopped at a frequency of 1900 kHz, yielding on average 6.7×10^6 ^{87}Rb atoms at 18 μK in the $|F = 2, m_F = 2\rangle$ state.

The dispersive imaging employs off-resonant light pulses propagating along the z direction, with an initial polarization along y. The Faraday effect leads to a rotation of the linear polarization by an angle $\theta \propto \tilde{n}$, with $\tilde{n}$ the column density [25]. The rotated light is sent through a polarizing beam splitter (PBS) and imaged on an electron multiplying charge coupled device (EMCCD) camera. This configuration realizes a "dark field" dispersive imaging technique [25,26]. The Faraday imaging sequence is realized with light that is blue detuned by $\delta = 2\pi \times (1200 \pm 1)$ MHz from the $F = 2 \rightarrow F' = 3$ transition. Over the spatial extent of the cloud, the intensity distribution is approximately uniform at a value of 0.5 mW/cm^2. The imaging light is monitored on a photodiode (PD) on the reflecting port of the PBS, and based on this signal, the imaging power is stabilized. $F1$ and $F2$ contain 50 and 100 rectangular pulses, respectively, with a cycle period of 7 ms. For each pulse, an image is acquired on the camera.

These images are evaluated in real time on a field programmable gate array (FPGA), which calculates the fraction of atoms to be removed. To apply feedback, the FPGA controls a synthesizer to generate rf pulses that induce the desired loss. A 10 s delay between $F1$ and $F2$ allows time for the loss pulses to be applied and for the cloud to thermalize. In the absence of applied loss, the cloud contains on average 4.3×10^6 atoms at 10 μK after $F2$. The temperature and atom number at $F2$ are the combined result of free evaporation and single-particle loss due to finite background pressure. Following $F2$, the trap is extinguished and the cloud is probed by resonant absorption imaging after 10 ms time of flight.

In the following, we evaluate the precision attained by Faraday imaging and then characterize the applied loss mechanism. Based on these results, we characterize the correlation between the measurements at $F1$ and $F2$, since this sets the limit for the precision that can be obtained by feedback. Finally, we show that atomic clouds below the shot noise level can be prepared by our feedback technique.

In the dark field Faraday imaging method, the light intensity on the camera scales with the "signal," defined as $S \equiv \sin^2 \theta$. We calculate this signal experimentally by $S = [I(\theta)/I_{ref} - 1]CS$, where I_{ref} is the intensity of the nonrotated light that leaks through the PBS due to its finite extinction ratio ("cube suppression") $CS \sim 10^{-3}$ [25]. The reference intensity I_{ref} is obtained from a region outside the atomic signal, and the baseline level of the camera is removed from $I(\theta)$ and I_{ref} by analyzing a masked region of the camera chip [27]. This procedure makes S independent of the EMCCD gain, which is prone to drift. The rotation angle, and hence the atomic density, can be obtained from $\theta = \arcsin(\sqrt{S})$, but, in practice, this is complicated by detection noise where θ is small, leading to negative values of S.

To avoid such technical issues on the FPGA, we calculate the signal sum Σ_S by summing S in a region of interest that encompasses the cloud. In the limit of small Faraday rotation angles, $S \approx \theta^2$, yielding $\Sigma_S \propto N^2/T$ for the thermal clouds in this work. We have characterized the scaling of Σ_S with N and T using results from absorption imaging. We find the observed functional dependence is well described by an empirical model motivated by the small angle dependence of Σ_S and that, to a good approximation, the fluctuations in temperature can be neglected [27]. Due to the quadratic dependence of Σ_S on N in the small angle limit, the relative fluctuations in the signal sum $\Delta\Sigma_S/\Sigma_S \approx 2\Delta N/N$ are approximately twice as large as those in N, making it a sensitive atom number probe. This approach allows us to exploit the high precision of Faraday imaging in combination with the accuracy of absorption imaging to determine the atom number.

The precision of this Faraday imaging technique can be obtained from an analysis of the fluctuations in Σ_S. Figure 2(a) shows Σ_S at $F1$ as a function of image number using an imaging pulse duration of $t = 0.66$ ms. The signal sum decreases over the 50 imaging pulses as a result of atom loss, primarily due to spontaneous scattering into
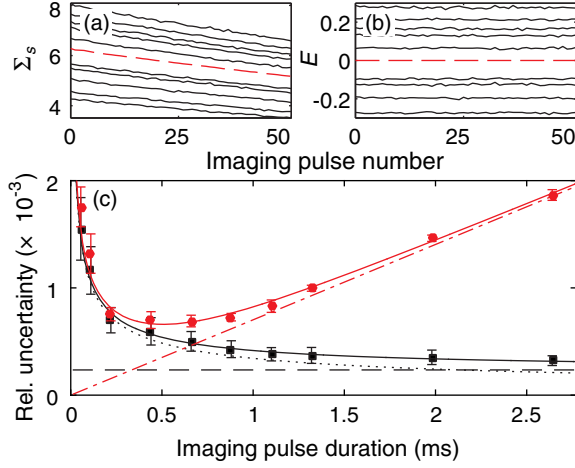
FIG. 2.   (a) Signal sum Σ_S vs image number for $F1$. Black lines show traces for 10 representative runs with imaging pulse duration $t = 0.66$ ms, and the dashed red line represents the mean trace $\langle \Sigma_S \rangle$ for the entire data set. (b) Error E for the same runs as (a). (c) Relative uncertainty vs t. Red circles represent $\langle \sigma_\Sigma \rangle$, the solid red line represents the fit of the imaging model σ_{Mod}, and the dash-dotted red line represents the mean atom loss contribution to σ_{Mod} fit $\propto t$. Black squares represent $\langle \sigma_E \rangle$, the solid black line represents the fit of σ_{Mod}, the dotted black line represents the light shot noise contribution to σ_{Mod} fit $\propto 1/\sqrt{t}$, and the dashed black line represents the constant technical noise contribution to σ_{Mod} fit. Error bars denote the standard error of the mean over several experimental runs.

untrapped electronic states. The fluctuations of the signal sum about this mean decay correspond to the light shot noise, the stochastic noise arising from atom loss, and potential technical noise. Since the mean atom loss is deterministic, one can remove the decay by normalizing Σ_S with its mean over several experimental runs and shift it to be centered on 0. Figure 2(b) shows this normalized signal $E \equiv \Sigma_S/\langle \Sigma_S \rangle - 1$, which we call the "error." We use the mean value of each error trace as a measure of the atom number in a given experimental run.

To characterize the imaging noise, we calculate the two-sample deviations $\Delta\Sigma$ and ΔE of Σ_S and E, respectively, for each trace. The relative uncertainty of Σ_S in a single imaging sequence is then given by the mean of $\Delta\Sigma$ over M imaging pulses $\sigma_\Sigma = (1/\sqrt{M-1})\langle(\Delta\Sigma/\Sigma_S)\rangle$, and equivalently for E it is $\sigma_E = (1/\sqrt{M-1})\langle\Delta E\rangle$. In total, the relative uncertainties are given by the mean value over several experimental runs denoted by $\langle \sigma_\Sigma \rangle$ and $\langle \sigma_E \rangle$.

Figure 2(c) shows the relative uncertainties of the signal sum $\langle \sigma_\Sigma \rangle$ and the error $\langle \sigma_E \rangle$ as a function of imaging pulse duration t. Initially, $\langle \sigma_\Sigma \rangle$ decreases as the imaging pulse duration is increased, but at 0.5 ms it reaches a minimum and then increases approximately linearly with t. The relative uncertainty $\langle \sigma_E \rangle$ shows the same initial behavior but does not increase for the range of t we consider. To understand this scaling, we use the following noise model

[30]: $\sigma_{\text{Mod}} = [At^{-1} + Bt + Ct^2 + D]^{1/2}$. The first term is the variance due to light shot noise; the second and third terms describe stochastic and mean atom loss, respectively; finally, the constant term D represents technical noise sources in the EMCCD, uncertainty in the imaging light detuning, and noise arising from the evaluation of S. The loss parameters are closely linked because they describe two effects of single atom loss: In the limit of low loss, $C = 2B^2$, where $Bt = N_0(1-p)/2$, and since $N_0 \sim 10^6$ and $p \simeq 1$, the noise term Bt describing stochastic atom loss is negligible compared to Ct^2. Fits to $\langle \sigma_\Sigma \rangle$ and $\langle \sigma_E \rangle$ are shown in Fig. 2(c). The fit to $\langle \sigma_\Sigma \rangle$ is dominated by the light shot noise and mean atom loss terms; this is characteristic of the two-sample deviation in an imaging method that induces significant atom loss [31]. The fitted values of A and C are consistent with estimates obtained from direct evaluation of the images. In contrast, $\langle \sigma_E \rangle$ is well fitted by only the light shot noise and technical noise, since the mean atom loss contribution has been removed by normalization. Indeed, for $t \lesssim 1$ ms, $\langle \sigma_E \rangle$ is approximately equal to the light noise, a fact we will employ in the following. At the optimal pulse duration of $t = 0.66$ ms, the relative uncertainty of E is 5×10^{-4}, which yields a relative uncertainty in the detected atom number of 2.5×10^{-4}. The imaging shows a similar performance at $F2$, for which the optimal imaging pulse duration is 0.55 ms. Thus, the Faraday imaging technique allows us to determine the atom number for clouds containing $\sim 5 \times 10^6$ atoms approximately a factor of 2 below the atom shot noise level.

To perform feedback, we require a mechanism to remove atoms from the cloud. It is important that this mechanism provides sufficiently fine resolution and does not drastically alter other parameters of the system such as the cloud's temperature. A convenient loss mechanism is realized by applying a variable number of fast rf pulses: These pulses transiently lower the trapping potential [32], whereby atoms are lost due to spilling. In general, we employ an rf corresponding to 95% of the trap depth U_0, with a pulse duration of 8.4 μs repeated every 50.4 μs. Since the elastic collision rate throughout the experiment after $F1$ is ~ 100 Hz, this pulse duration is short compared to the mean time between collisions. These parameters are chosen to achieve a very small fractional loss of $\sim 10^{-5}$ per pulse, thus providing fine digital resolution. For example, to remove 10% of the atoms, we apply $\sim 10^4$ loss pulses.

Based on these results, we characterize the level of correlation between the measurements at $F1$ and $F2$. The fluctuations of this correlation set the limit for the precision that can be achieved with feedback, since the feedback strength for a desired result at $F2$ is calculated from the signal obtained at $F1$. The correlation is measured for several fixed applied loss settings. Figure 3 (inset) shows the outcome of such a measurement in terms of the mean measured error at $F1$ and $F2$, where the error varies by $\pm 40\%$ due to the natural fluctuations of the experiment;
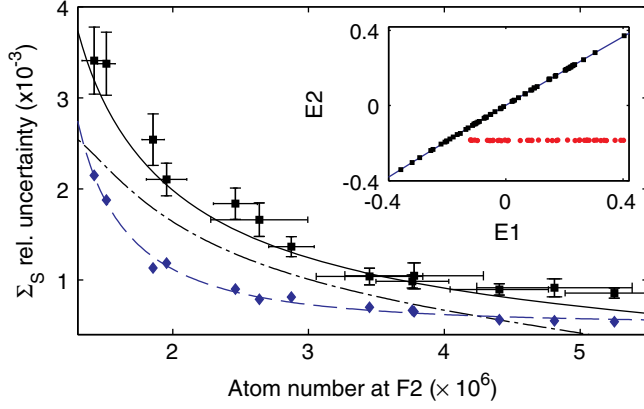
FIG. 3. The black squares represent the signal sum relative uncertainty vs atom number at $F2$, the solid black line represents the total noise model, the blue diamonds represent the imaging noise contribution, the dashed blue line represents the fit $\propto 1/N$ to imaging noise data, and the dash-dotted black line represents the stochastic atom loss noise contribution $\sqrt{(1-p)/\langle N \rangle}$. Error bars were obtained by bootstrapping the data set. Inset: Correlation of error at $F1$ and $F2$. The black squares represent the correlation data with no applied loss, the blue line represents the quadratic fit to correlation data, and the red circles represent the feedback stabilized points.

this corresponds to a $\pm 20\%$ span in atom number. To evaluate how well $E1$ and $E2$ are correlated, we fit a quadratic function to the data and subtract this fit from the data. The relative fluctuations between $E1$ and $E2$ are then determined by taking the two-sample deviation over successive runs of the experiment to remove slow drifts in the apparatus such as changes in the trap bottom.

Figure 3 shows the relative uncertainty in the detected total signal at $F2$ for a number of fixed loss settings, corresponding to several mean numbers of atoms remaining in the trap. These correlation data allow for an analysis of the inherent noise sources. The data are well described by contributions from the imaging noise and from the stochastic noise due to the atom loss between the two imaging series. The imaging noise is given by the light shot noise and technical noise contributions in $F1$ and $F2$ (corresponding to $\langle \sigma_E \rangle$ for each imaging series) added in quadrature. It has been fitted by a function $\propto 1/N$, which we expect from error propagation [27]. For the stochastic atom loss contribution, the relative uncertainty in the number of atoms remaining in the cloud $\sqrt{(1-p)/\langle N \rangle}$ is shown, which has been transformed into the signal sum using the model linking Σ_S to N and T. The total noise, given by the quadrature sum of these contributions shows very good agreement with the experimental data. This crucial result shows that there are no unknown technical noise sources that influence the number of atoms between $F1$ and $F2$, which is a prerequisite to perform feedback below the shot noise level.

The achievements outlined above allow us to turn to the active stabilization of the atom number by feedback. Based on the average error in $F1$, the fraction of atoms removed from the cloud is controlled by varying the number of applied loss pulses. To generate a reference signal $\langle \Sigma_S^{\mathrm{ref}} \rangle$ for this feedback, we typically cycle the experiment with no applied loss for ~ 50 runs. In subsequent experimental runs with feedback, $E1' \equiv \Sigma_S/\langle \Sigma_S^{\mathrm{ref}} \rangle - 1$ is determined at $F1$, and the number of rf loss pulses N_{Loss} is calculated using a cubic feedback function $N_{\mathrm{Loss}} = gE1'(1 + qE1' + cE1'^2) + d$. This function approximates the atom loss that is exponential in the number of applied loss pulses. The linear g, quadratic q, and cubic c gain parameters as well as the offset d are determined by evaluating the outcome over several experimental runs for a trial set of feedback parameters and iterating [27]. Figure 3 (inset) shows a data set where the feedback parameters have been optimized to achieve a stabilized value of $E2$ for all initial errors $E1'$ that are larger than the target value. In this case, the stabilized atom number is $\sim 90\%$ of the mean atom number of the free running experiment.

Finally, the uncertainty in the stabilized sample is characterized to verify that the feedback mechanism does not add additional noise and that stabilization below the shot noise level can be achieved. We take the two-sample deviation of $E2$ over successive runs of the experiment for several target atom numbers. The relative uncertainty is shown as red circles in Fig. 4. For clouds prepared at $N \gtrsim 2.5 \times 10^6$, the feedback achieves a level of stabilization that is limited by the fundamental noise imposed by the single-particle loss mechanism, showing that the feedback does not induce additional noise. These clouds are stabilized at or below the atom shot noise level $1/\sqrt{N}$.

For samples stabilized to lower atom numbers, the observed noise exceeds the correlation data and the noise model. For $N < 2.5 \times 10^6$, we remove more than 60% of the atoms from the cloud, whereby the modeling of the exponential loss by the cubic feedback function becomes less accurate. Additionally, the passive stability of the
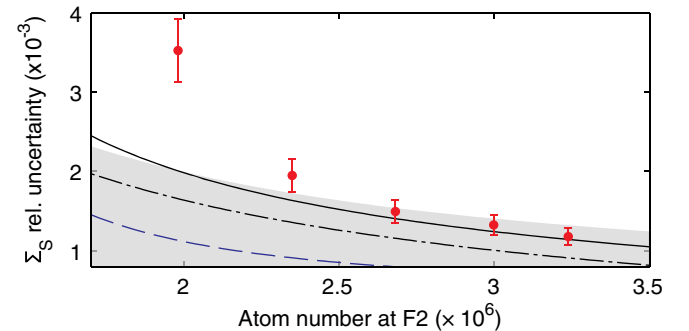

FIG. 4. The red circles represent the signal sum relative uncertainty vs atom number at $F2$ for feedback stabilized clouds. Other lines same as Fig. 3. The shaded region represents the interval where the relative uncertainty in the signal sum lies below the shot noise level, i.e., $1/\sqrt{N}$ expressed as signal sum [27].

apparatus, such as drifts in the trap bottom, becomes a significant source of noise in the stabilized atom number for high fractional loss.

In conclusion, we have prepared number stabilized atom clouds through feedback. An investigation of our nondestructive imaging technique yielded an uncertainty in the measured atom number that was about a factor of 2 smaller than the atom shot noise level. The precision of correlation measurements within an experimental realization was entirely determined by the removed fraction of atoms, demonstrating the absence of technical noise sources between the imaging series. Finally, feedback based on a nondestructive measurement allowed for stabilization at or below the level of $1/\sqrt{N}$ for large atom clouds with $N \gtrsim 2.5 \times 10^6$.

The potential of our technique can be further exploited by employing multiple feedback steps and improved atom number determination. A second feedback step requiring only a small removal of atoms would strongly reduce the induced noise, whereby the imaging noise would become the limiting factor. To improve the Faraday imaging, more sophisticated atom number estimators will be used to better exploit the information from multiple images. Additionally, the atom number decay due to imaging itself could realize the final feedback step [31], in which case an algorithm such as a Kalman filter would stop the imaging series when the target atom number is detected. However, even at the present level, our technique can make a considerable contribution to improve the precision of current [11] or nonclassical [12–15] atom interferometers.

*Corresponding author.
hilliard@phys.au.dk

[1] J. Zhang, Y.-x. Liu, R.-B. Wu, K. Jacobs, and F. Nori, arXiv:1407.8536.

[2] C. Sayrin, I. Dotsenko, X. Zhou, B. Peaudecerf, T. Rybarczyk, S. Gleyzes, P. Rouchon, M. Mirrahimi, H. Amini, M. Brune, J.-M. Raimond, and S. Haroche, Nature (London) **477,** 73 (2011).

[3] H. J. Briegel, D. E. Browne, W. Dur, R. Raussendorf, and M. Van den Nest, Nat. Phys. **5,** 19 (2009).

[4] J. J. Hope and J. D. Close, Phys. Rev. Lett. **93,** 180402 (2004).

[5] N. V. Morrow, S. K. Dutta, and G. Raithel, Phys. Rev. Lett. **88,** 093003 (2002).

[6] B. Julsgaard, J. Sherson, J. I. Cirac, J. Fiurásek, and E. S. Polzik, Nature (London) **432,** 482 (2004).

[7] K. C. Cox, G. P. Greve, J. M. Weiner, and J. K. Thompson, Phys. Rev. Lett. **116,** 093602 (2016).

[8] T. Vanderbruggen, R. Kohlhaas, A. Bertoldi, S. Bernon, A. Aspect, A. Landragin, and P. Bouyer, Phys. Rev. Lett. **110,** 210503 (2013).

[9] R. Kohlhaas, A. Bertoldi, E. Cantin, A. Aspect, A. Landragin, and P. Bouyer, Phys. Rev. X **5,** 021011 (2015).

[10] N. Behbood, G. Colangelo, F. Martin Ciurana, M. Napolitano, R. J. Sewell, and M. W. Mitchell, Phys. Rev. Lett. **111,** 103601 (2013).

[11] A. D. Ludlow, M. M. Boyd, J. Ye, E. Peik, and P. O. Schmidt, Rev. Mod. Phys. **87,** 637 (2015).

[12] C. Gross, T. Zibold, E. Nicklas, J. Estève, and M. K. Oberthaler, Nature (London) **464,** 1165 (2010).

[13] M. F. Riedel, P. Böhi, Y. Li, T. W. Hänsch, A. Sinatra, and P. Treutlein, Nature (London) **464,** 1170 (2010).

[14] B. Lücke, M. Scherer, J. Kruse, L. Pezzè, F. Deuretzbacher, P. Hyllus, O. Topic, J. Peise, W. Ertmer, J. Arlt, L. Santos, A. Smerzi, and C. Klempt, Science **334,** 773 (2011).

[15] H. Strobel, W. Muessel, D. Linnemann, T. Zibold, D. B. Hume, L. Pezzè, A. Smerzi, and M. K. Oberthaler, Science **345,** 424 (2014).

[16] L. Pezzé and A. Smerzi, Phys. Rev. Lett. **110,** 163604 (2013).

[17] J. Zeiher, P. Schauß, S. Hild, T. Macrì, I. Bloch, and C. Gross, Phys. Rev. X **5,** 031015 (2015).

[18] S. Whitlock, C. F. Ockeloen, and R. J. C. Spreeuw, Phys. Rev. Lett. **104,** 120402 (2010).

[19] A. Itah, H. Veksler, O. Lahav, A. Blumkin, C. Moreno, C. Gordon, and J. Steinhauer, Phys. Rev. Lett. **104,** 113001 (2010).

[20] J.-B. Béguin, E. M. Bookjans, S. L. Christensen, H. L. Sørensen, J. H. Müller, E. S. Polzik, and J. Appel, Phys. Rev. Lett. **113,** 263603 (2014).

[21] F. Serwane, G. Zürn, T. Lompe, T. B. Ottenstein, A. N. Wenz, and S. Jochim, Science **332,** 336 (2011).

[22] C.-S. Chuu, F. Schreck, T. P. Meyrath, J. L. Hanssen, G. N. Price, and M. G. Raizen, Phys. Rev. Lett. **95,** 260403 (2005).

[23] B. J. Sawyer, A. B. Deb, T. McKellar, and N. Kjærgaard, Phys. Rev. A **86,** 065401 (2012).

[24] N. G. van Kampen, *Stochastic Processes in Physics and Chemistry*, 3rd ed. (Elsevier, Amsterdam, 2007).

[25] M. Gajdacz, P. L. Pedersen, T. Mørch, A. J. Hilliard, J. Arlt, and J. F. Sherson, Rev. Sci. Instrum. **84,** 083105 (2013).

[26] C. C. Bradley, C. A. Sackett, and R. G. Hulet, Phys. Rev. Lett. **78,** 985 (1997).

[27] See Supplemental Material at http://link.aps.org/supplemental/10.1103/PhysRevLett.117.073604, which includes Refs. [25,28,29], for further details.

[28] W. Ketterle and N. J. Van Druten, Adv. Atom. Mol. Opt. Phys. **37,** 181 (1996).

[29] B. Efron, Ann. Stat. **7,** 1 (1979).

[30] D. B. Hume, I. Stroescu, M. Joos, W. Muessel, H. Strobel, and M. K. Oberthaler, Phys. Rev. Lett. **111,** 253001 (2013).

[31] A. J. Hilliard, Y. H. Fung, P. Sompet, A. V. Carpentier, and M. F. Andersen, Phys. Rev. A **91,** 053414 (2015).

[32] A. del Campo and J. G. Muga, Phys. Rev. A **78,** 023412 (2008).